ACS APPLIED MATERIALS & INTERFACES

Research Article

www.acsami.org

Release of Ceria Nanoparticles Grafted on Hybrid Organic–Inorganic Films for Biomedical Application

Alessandra Pinna,[†] Cristiana Figus,[†] Barbara Lasio,[†] Massimo Piccinini,[‡] Luca Malfatti,[†] and Plinio Innocenzi*[,†]

[†]Laboratorio di Scienza dei Materiali e Nanotecnologie, LMNT-D.A.D.U., Università di Sassari and CR-INSTM, Palazzo Pou Salit, Piazza Duomo 6, 07041 Alghero, Sassari, Italy

[‡]Imaging Laboratory, Porto Conte Ricerche, SP 55 Porto Conte-Capo Caccia km 8,400, Loc. Tramariglio, 07041 Alghero (Sassari), Italy

Supporting Information

ABSTRACT: The controlled release of nanoparticles from a hybrid organic–inorganic surface allows for developing several applications based on a slow delivery of oxygen scavengers into specific environments. We have successfully grafted ceria nanoparticles on a hybrid film surface and tested their release in a buffer solution; the tests have shown that the particles are continuously delivered within a time scale of hours. The hybrid film has been synthesized using 3-glycidoxypropyltrimethoxysilane as precursor alkoxide; the synthesis has been performed in highly basic conditions to control the polycondensation reactions of both organic and inorganic networks via controlled aging of the solution. Only films prepared from aged solutions are able to graft ceria nanoparticles on their surface. The ceria nanoparticles have been characterized by X-ray diffraction, transmission electron microscopy and UV–vis spectroscopy, the hybrid films have been analyzed by Fourier transform infrared spectroscopy, atomic force microscopy and Raman spectroscopy. Raman imaging has been used for the release test. The hybrid film–ceria nanoparticles system fulfils the requirements of optical transparency and stability in buffer solutions which are necessary for biomedical applications.

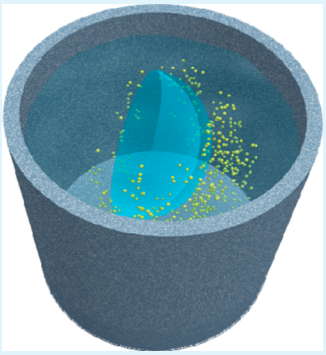

KEYWORDS: *ceria nanoparticles, organic–inorganic hybrid films, radical scavenger, contact lens*

INTRODUCTION

Hybrid organic–inorganic materials synthesized using 3-glycidoxypropyltrimethoxysilane (GPTMS) as the organically modified alkoxide have a very peculiar structure which is given by the presence of a terminal epoxy group in the precursor alkoxide.[1] The opening of the epoxides in controlled conditions allows the formation of an organic polymeric structure, basically poly(ethylene oxide) chains whose extent depends on the synthesis parameters.[2−6] If the formation of the inorganic silica backbone is faster than the organic condensation, the growth of long polymeric chains is hindered.[2−5] In general, within this frame, the sol–gel chemistry is flexible enough to allow a wide tuning of the final structure; if the synthesis is pushed to some limit conditions, such as in a very basic environment,[7] the polycondensation and polymerization reactions are slowed down enough to allow forming bridged silsesquioxane compounds which self-organize into ordered layered structures.[8,9] The role played by the epoxide is not only a structural one, because the surface properties are also strongly affected; when the epoxides are closed, the hybrid surface is relatively more hydrophobic, whereas with the increase in the amount of reacted epoxides, the material becomes increasingly hydrophilic.[10] The GPTMS hybrids on the other hand show also excellent optical properties and have been used to prepare different types of photonic devices, such as planar waveguides,[11,12] optical limiters,[13−15] and nonlinear optical materials.[16−18] The optical transparency and the antiscratch properties exhibited by GPTMS hybrids have also made this material a successful product in the market for optical contact lenses.[19−21] Beside these successful cases, we have taken the challenge to develop a new type of GPTMS material for potential application as functional contact lenses with advanced properties, which should be able not only to correct the vision problems of the eyes, but that could potentially play an active role on protecting them from degeneration phenomena.

Quite recently, it has been shown that cerium oxide nanoparticles are powerful scavengers of toxic reactive oxygen intermediates, which are responsible of light-induced degeneration of photoreceptor cells in eyes.[22] These properties of ceria nanoparticles are correlated to the presence of oxygen vacancies or defects in the lattice structure which make ceria an ideal free radical scavenger with antioxidant action.[23] When cerium oxide is produced in form of nanoparticles, the surface area dramatically increases and greater oxygen exchange and redox reactions may occur. Cerium oxide can also act as oxygen buffers because of its high redox capacity, which increases with

Received: April 24, 2012
Accepted: July 3, 2012
Published: July 3, 2012

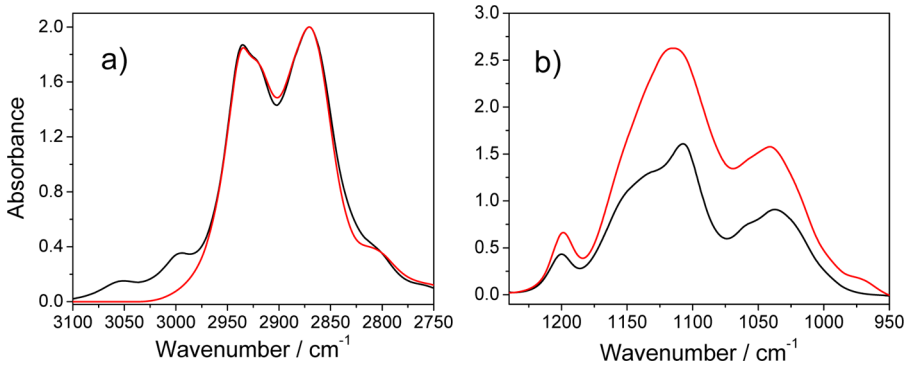

Figure 1. (a) FTIR absorption spectra in the 3100−2750 cm^{-1} and (b) in the 1240−950 cm^{-1} range of GPTMS films prepared from a fresh sol (black line) and 6 days aged sol (red line).

decreasing particle size, as extensively reported in the literature.[24,25]

Topical delivery of ceria nanoparticles through eye drops, which is the simplest ophthalmic option, is not very efficient and in some cases some serious side effects[26,27] can arise. An alternative is the delivery through soft contact lenses which should slowly release the nanoparticles as an ophthalmic drug delivery system. The very basic idea is to graft ceria nanoparticles on the surface of a hybrid material based on GPTMS, which is a common precursor for contact lenses and to activate a controlled release when the material is immersed in a physiological solution. To reach this goal, however, it is necessary that the nanoparticle size is small enough, the loading sufficiently low, and that the particle-grafted material maintains a high optical transparency. We report in this article an example of GPTMS hybrid whose surface is covered with ceria nanoparticles that are able to be slowly released when immersed in a buffer solution.

EXPERIMENTAL SECTION

1.1. Synthesis of Ceria Nanoparticles. Cerium(III) nitrate hexahydrate ($Ce(NO_3)_3{\cdot}6H_2O$, ABCR 99.9%), 1-hexadecyl-trimethylammonium bromide (CTAB 98%, ABCR), 2-propanol (99.7%, Carlo Erba), 1 M hydrochloric acid (HCl, Aldrich), 5 M aqueous ammonia (NH_4OH, Aldrich), 3-glycidoxypropyltrimethoxysilane (GPTMS, Aldrich 98%), sodium hydroxide (pellets 98%, Carlo Erba), ethanol (EtOH, Aldrich 99.5%), acetone (Aldrich 99.5%) and phosphate buffered saline 10X concentrate (Sigma Aldrich) were used as received without further purification; p-type boron-doped silicon wafers, silica and soda-lime glass slides were employed as substrates for film deposition.

The synthesis to obtain ceria nanoparticles employed a cationic surfactant (1-hexadecyl-trimethylammonium bromide), $Ce(NO_3)_3$ and NH_4OH as inorganic precursors; 7 g of $Ce(NO_3)_3{\cdot}6H_2O$ was dissolved and 0.5 cm^3 hydrochloric acid was added in 20 cm^3 of 2-propanol and left under stirring until a homogeneous solution has been obtained. In a separate vial, 2 g of CTAB and 0.5 cm^3 of HCl were dissolved in 20 cm^3 of 2-propanol and left under stirring for 5 min. The CTAB solution was then added, dropwise, to the $Ce(NO_3)_3$ solution under stirring, immediately after 14 cm^3 of NH_4OH(aq) were added to the mixture to form a precipitate that was exposed to microwaves (4 times at 600 W for 10 s), washed with water and centrifuged at 10000 rpm. A light yellow milky dispersion was obtained and diluted with water to reach a concentration of 0.08 g CeO_2 per cm^3 (ceria stock suspension).

1.2. Synthesis of Hybrid Organic−Inorganic Films. The precursor sol, was prepared by addition of GPTMS (10 cm^3) to a NaOH aqueous solution (4 cm^3, 1.85 M, pH 14) under stirring. The molar ratio of the components was set to GPTMS:H_2O:NaOH = 1:5:0.167. Immediately after the preparation, the precursor sol was left in an open vessel at 25 °C and 40% RH for 30 min to allow the evaporation of methanol, which is a byproduct of the sol−gel reactions; after this time, the sol was left under stirring for 12 h at 25 °C in a closed vial and then aged up to 6 days at 25 °C without stirring. This sol was used for the deposition of hybrid films by spin-coating on silicon and silica substrates using a rotation speed of 5000 rpm for 20 s; the substrates were cleaned with water, acetone and ethanol. The films were deposited using different aging time of the sol; after the deposition, the films were thermally treated at 100 °C for 48 h.

1.3. Functionalization of Hybrid Organic−Inorganic Films with Ceria Nanoparticles. The anchoring of ceria nanoparticles on the films was reached by a postgrafting method involving the incubation, in Petri dishes, of the hybrid organic−inorganic films immersed in 20 cm^3 of ethanol containing 0.5 cm^3 of ceria stock suspension for 48 h, after which the hybrid films were washed with ethanol and dried on the open air.

1.4. Release of Ceria Nanoparticles from the Film Surface. The hybrid organic−inorganic films containing ceria nanoparticles were incubated for 1, 5, and 17 h in a 20 cm^3 volume vial of 1X phosphate buffer solution of pH 7.4. The films were then immersed in the buffer and after the incubation time were dried in air; the ceria release from hybrid organic−inorganic films was monitored by Raman spectroscopy.

1.5. Characterization of Hybrid Organic−Inorganic Films Containing Ceria Nanoparticles. Fourier transform infrared (FTIR) measurements were performed using a Vertex 70 Bruker spectrophotometer in the 400−4000 cm^{-1} range with a resolution of 4 cm^{-1} on films deposited on a silicon wafer; silicon was used for the background reference. The FTIR spectra were analyzed in the 3100−2750 cm^{-1} regions correcting the baseline by subtracting a concave rubberband with OPUS 7 software.

Optical properties have been measured by a Nicolet Evolution 300 UV−vis spectrophotometer working in intelliscan mode, silica glass has been used as background reference.

X-ray diffraction (XRD) patterns of CeO_2 nanoparticles and CeO_2 nanoparticles grafted on hybrid films were collected using a Bruker D8 discover instrument in grazing incidence geometry with a Cu K_α line (λ = 1.54056 Å); the X-ray generator worked at a power of 40 kV and 40 mA. The patterns were recorded in 2θ ranging from 25 to 75° with a step size of 0.02° and a scan speed of 0.5 s by a repetition mode for 12 h until maximization of the signal-to-noise ratio. The XRD data were analyzed with the MAUD software according to the Rietveld method; average crystallite size and lattice strain were separated from the total broadening assuming a dependence of microstrain from the reflection order following an isotropic model.[28]

An atomic force microscope (NT-MDT Ntegra) was used to analyze the topography of the samples. Surface was measured at 0.5−1 Hz scan speed in semicontact mode, using a silicon tip with nominal resonance frequency of 130 kHz, 4.4 N m^{1-} force constant, and 10 nm typical curvature radius. Measures of surface roughness were performed by using the WSxM 5.0 Develop 3.2 software.[29]

Transmission electron microscopy (TEM) images were obtained using a JEOL 200CX microscope equipped with a tungsten cathode operating at 200 kV. Prior to observation, a fragment of the sample was removed from the substrate and deposited on a carbon-coated copper grid after gentle grinding on an agate mortar.

A Bruker Senterra confocal Raman microscope working with a laser excitation wavelength of 532 nm at 50 mW of nominal power was used for Raman characterization. The 100× objective was selected and an array of 6 × 8 points was defined to cover an area of 15 × 20 μm with a step of 2.5 μm. Each spectrum of the map was obtained by averaging 5 acquisitions of 5 s. The Raman spectra were collected in a region of 5 μm^2 where ceria nanoparticles were previously identified by optical microscope. To monitor the ceria release, 3 points were measured in the selected region before and after immersion of the sample in the phosphate buffer. The spectra were averaged in the 425–490 cm^{-1} range after rubberband baseline subtraction; OPUS 7 software was used for data manipulation. Every point of the release experiment were obtained by using different samples from the same batch; each sample was immersed for the selected delivery time. Before every release test the Raman reference spectra (time 0) were collected and compared to those ones after the test; finally the measured spectra have been normalized using the Raman spectra before the release test.

2. RESULTS AND DISCUSSION

2.1. GPTMS Films. The GPTMS hybrid films have been synthesized in very basic conditions (pH 14) which promote a strong hydrolysis of the alkoxides but hinder a complete inorganic condensation and the opening of the epoxides.[30] Films prepared with a fresh sol show that the epoxides remain largely unreacted while they disappear in coatings obtained from aged sols. We have used infrared analysis to characterize the hybrid material structure, Figure 1a shows the FTIR absorption spectra in the 3100–2750 cm^{-1} range of GPTMS films prepared from a fresh sol (black line) and 6 days aged sol (red line). This wavenumber interval corresponds to the CH_2 stretching region with the two main bands around 2920 and 2880 cm^{-1} which are assigned to CH_2 antisymmetric (CH_2, ν_{asym}) and CH_2 symmetric stretching (CH_2, ν_{sym}), respectively (spectra a and b in Figure 1 have been normalized with respect to the band at 2850 cm^{-1}; baseline has been obtained using a

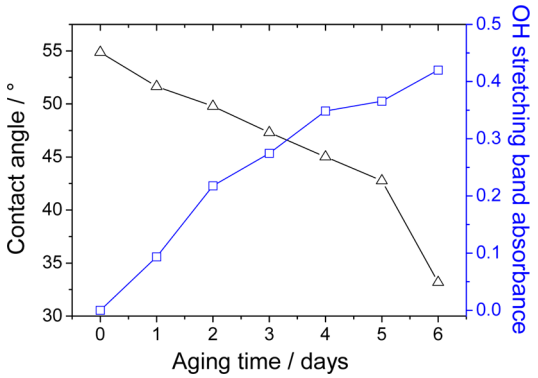

Figure 2. Change of contact angle and OH stretching band absorbance (~3430 cm^{-1} band) in GPTMS films as a function of aging time. The lines are a guide for the eye.

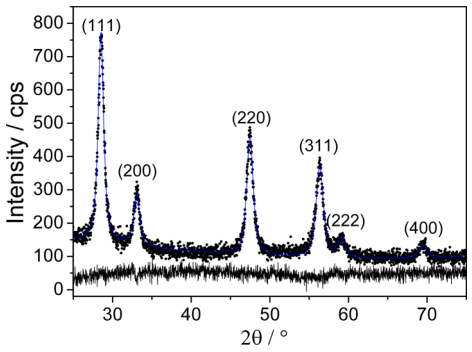

Figure 3. XRD pattern (black dots) of ceria nanoparticles after microwaves treatment; the Rietveld fit is shown with a continuous blue line. At the bottom of the figure is reported the curve of residuals $I_{calcs}^{1/2} - I_{exp}^{1/2}$ (black line).

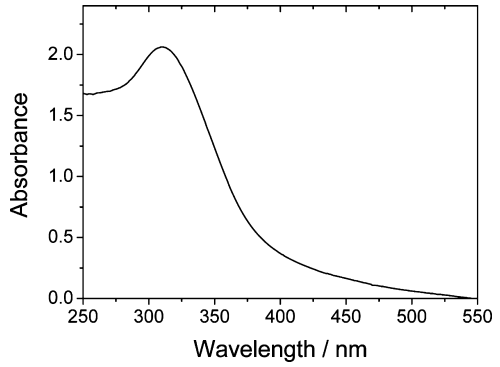

Figure 4. UV–vis absorption spectrum in the 250–550 nm interval of an aqueous dispersion of CeO_2 nanoparticles.

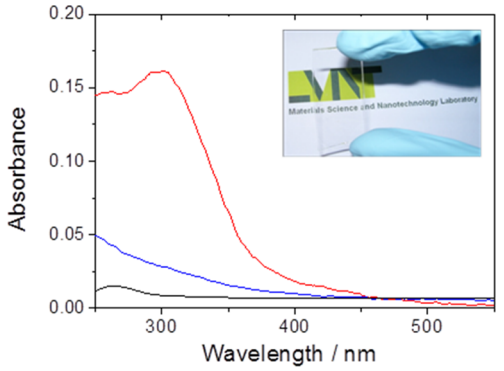

Figure 5. UV–vis absorption spectra in the 250–550 nm range of hybrid films; GPTMS with open epoxides (6 days aging, red line) grafted with CeO_2 NPs, GPTMS with closed epoxides (fresh sol, blue line) grafted with CeO_2 NPs, reference spectra of a GPTMS hybrid film (6 days aged, black line). The inset shows the optical image of the 6 days aged film with grafted ceria nanoparticles.

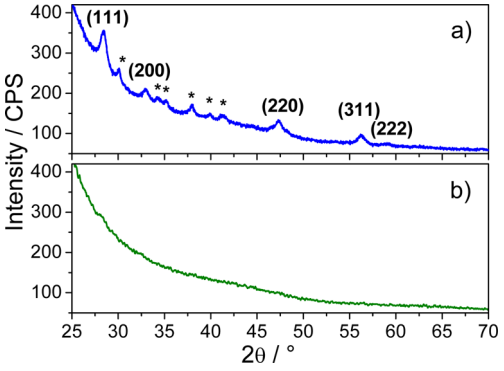

Figure 6. (a) XRD pattern of ceria nanoparticles grafted on the GPTMS hybrid film prepared from an aged sol (open epoxides) and (b) from a fresh sol (closed epoxides). The diffraction peaks from the silicon substrate are indicated by *.

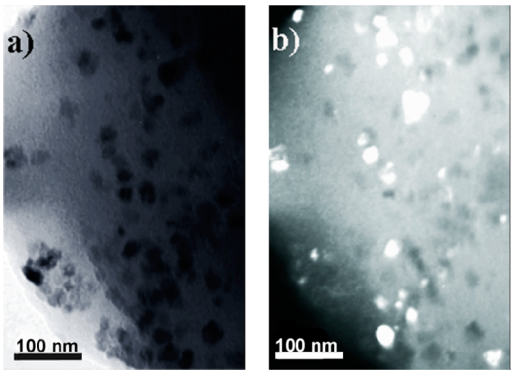

Figure 7. TEM images of a fragment taken from a GPTMS hybrid film with grafted CeO_2 NPs with open epoxides (prepared from the coating sol aged for 6 days). a) Bright and b) dark field image.

rubberband function). These two main bands overlap with two absorption peaks, in particular at 3050 and 2955 cm^{-1}, which are attributed to stretching modes of terminal CH_2 groups of the epoxides in GPTMS; another overlapped band at smaller wavenumbers around 2800 cm^{-1} is also assigned to epoxides.[31] These bands disappear in the aged sol sample, indicating that the epoxides full reacted upon aging; with the increase of sol aging time we also observed an increase, both in intensity and area, of the wide OH stretching band peaking around 3430 cm^{-1} (not shown in Figures). The same FTIR spectra in the region of Si−O−Si antisymmetric stretching mode[32] (1240−950 cm^{-1} range, Figure 1b) indicate that the silica condensation is higher in the 6 days aged sol with respect to the fresh one. The wide intense band peaking around 1110 cm^{-1} (Si−O−Si, ν_{asym}), in fact, increases in intensity and the shoulder at 1150 cm^{-1} due to unreacted alkoxy groups disappears.[32] These changes clearly show that in films prepared from an aged sol the silica backbone is much more interconnected.

The extent of the condensation reactions affects also the hybrid film surface which becomes more and more hydrophilic in the samples prepared using a sol of longer aging times; the contact angle of the surface decreases from 55° in fresh sol films to around 32° in 6 days aged sol samples (Figure 2). A relative comparison of the contact angle change as a function of the amount of hydroxyls shows that there is a good correlation between the decrease in contact angle and the increase in hydroxyls content with sol aging. The amount of hydroxyls has been evaluated on the ground of the OH stretching band[32] intensity around 3430 cm^{-1} from spectra normalized with respect to the band at 2850 cm^{-1} (See Supporting Information, Figure S1). The trend shown by the OH content is quite counterintuitive, because it should be expected that the amount of silanols decreases with the increase in aging time and the proceed of the polycondensation reactions. In this case, however, the presence of the epoxy groups which are hydrophobic changes the scenario; the epoxides at this high pH value (~14) do not open all at the same time but slowly react with the aging time. When more and more epoxides react, they form a more hydrophilic environment, which is due to an increase of hydroxyl groups; this change also strongly affects the surface, which becomes more hydrophilic, as shown by the decrease in contact angle (Figure 2).

2.2. Synthesis of Ceria Nanoparticles. The synthesis of ceria nanoparticles that we have employed allows obtaining a good control of dimension and size distribution of the particles. The XRD pattern in the angular range 25−75° of the CeO_2 NPs after the microwave treatment (Figure 3), shows diffraction peaks that correspond to the (111), (200), (220), (311), (222), and (400) planes for the cubic fluorite structure of CeO_2 cerianite (JCPDS: 34−0394). The patterns have been analyzed according to the Rietveld method,[33] using the program MAUD[28] running on a personal computer. The Rietveld fit gives 14.55 ± 2.3 nm for the crystallite size and 0.54 ± 0.37 nm for lattice parameter *a*, which is the same as the one reported for CeO_2 in the standard data (a = 0.5411 nm, space group $Fm3m$) (JCPDS: 34−0394).

The aqueous dispersion of CeO_2 NPs has been characterized by UV−vis spectroscopy; Figure 4 shows the UV−vis absorption spectrum in the 250 - 550 nm interval, the concentration of ceria NPs is 80 mg mL^{-1}. The sample shows a strong absorption with a well-defined absorbance peak at around 310 nm (4 eV). The absorption in this region is due to the charge-transfer transitions from O 2p to Ce 4f, which overruns the f−f spin−orbit splitting of the Ce 4f state.[34−38] As reported in previous works, the broad absorption from 310 nm up to 500 nm is likely due to Rayleigh scattering of the nanoparticles in solution.[39]

2.3. Grafting of CeO_2 Nanoparticles on GPTMS Films. The third step of the synthesis has been the grafting of the nanoparticles on the surface of GPTMS films. We have specifically developed this hybrid-CeO_2 NPs system well keeping in mind that some peculiar properties are required. The surface of the film should allow an efficient and robust grafting of the NP_S but, at the same time, the system should

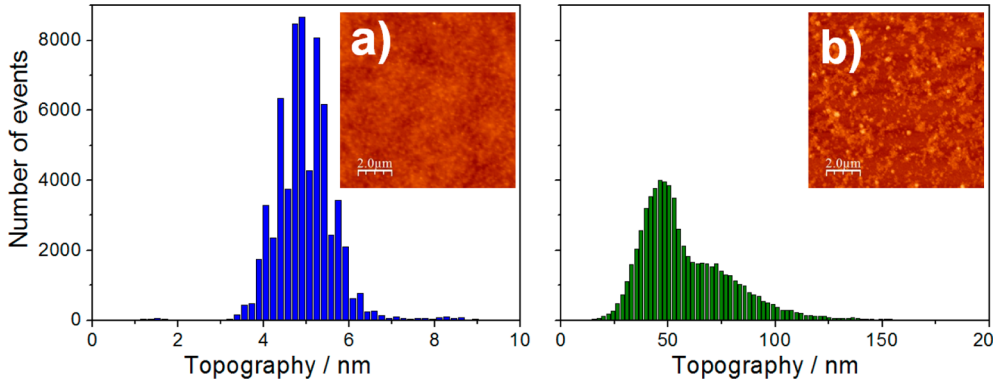

Figure 8. AFM images of the GPTMS film (a) before and (b) after ceria grafting. The surface roughness topography of the two images is reported as inset.

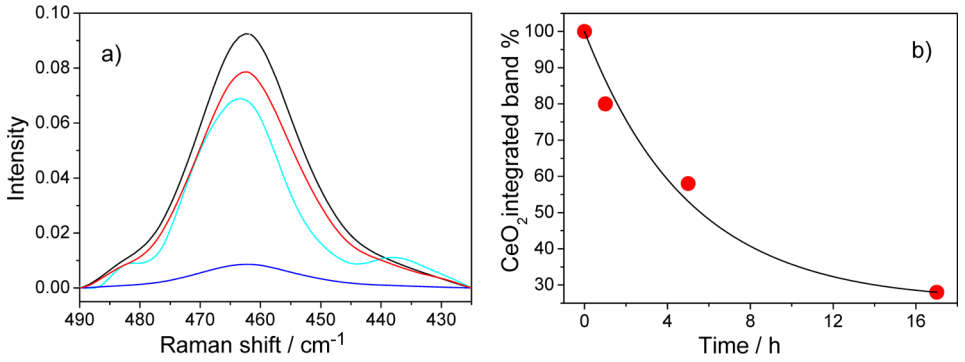

Figure 9. (a) Raman spectra in the 490−425 cm^{-1} range of ceria nanoparticles grafted on GPTMS film before (black line) and after a release test of 1 h (red line), 5 h (cyan) and 17 h (blue line) in phosphate buffer at pH 7.4. (b) Variation in ceria Raman integrated band area as a function of releasing test time (in hours); the black line is the exponential decay fit curve. The ceria nanoparticles concentration in water solution is 80 mg cm^{-3}.

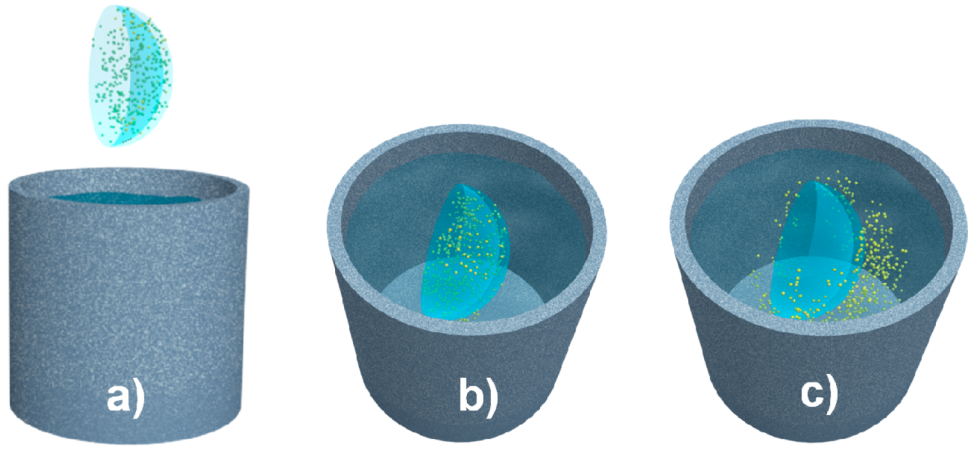

Figure 10. (a) Grafted ceria nanoparticles when the sample is (b) immersed in a buffer solution are (c) slowly released.

response when immersed in a buffer solution by slowly releasing the particles and maintaining an optical transparency of the film. We have tested the result of the grafting process by several techniques, UV−vis, XRD, TEM and AFM. Figure 5 shows the UV−vis absorption spectra in the 250−550 nm range of hybrid films with grafted CeO_2 NPs in the case of GPTMS with open epoxides (6 days aging, red line), and GPTMS with closed epoxides (fresh sol, blue line), GPTMS hybrid film spectrum obtained from 6 days aged sol is also reported as reference (black line). The spectra show that the grafting process is effective only in the case of GPTMS films which have been prepared from an aged sol and whose epoxides have been opened; the UV−vis spectrum exhibits in fact the typical signature of the ceria NPs as can be estimated by comparing this spectrum with that one in Figure 3 of pure ceria. On the other hand, the hybrid reference film with open epoxides shows a high optical transparency while the sample with closed epoxides has only a not-structured small diffuse absorption from 350 to 250 nm, very likely due to a small amount of grafted particles. To confirm the successful grafting of ceria nanoparticles on the GPTMS hybrid film prepared from the aged sol, we have performed XRD analysis at grazing incidence on the coating. The sample shows a diffraction pattern which is assigned to cerianite NPs (Figure 6a), in accordance to XRD characterization of the ceria NPs in Figure 3; grafting the nanoparticles using the same protocol on the GPTMS fresh sol film does not work and no diffraction patterns have been recorded from this sample (Figure 6b). The XRD and UV−vis spectra are well in agreement each other and indicate that grafting of ceria NPs is possible only on samples prepared from aged sols (open epoxide).

We have also taken some fragments from the surface of the films to be analyzed by TEM; the bright and dark field images are shown in images a and b in Figure 7, respectively. The ceria NPs appear well distributed within the sample and the dimension is in the range between 20 and 50 nm.

The samples surface has been analyzed by AFM, as shown Figure 8**a** and **b** respectively; the surface roughness topography of the GPTMS film before and after ceria grafting is also shown as inset in the same figures. The bare GPTMS surface appears smooth with a calculated root-mean-square (rms) of 0.73 nm, while after nanoparticles grafting the rms value increases to 22.31 nm. It is also interesting to observe that the topography of the film surface after particle grafting seems basically composed by a bimodal distribution which is given by two Gaussian components one centered around 50 nm and another one around 75 nm; this should indicate that the particles are distributed quite homogeneously on the film surface and some particles get closer to form small clusters, which increase the surface roughness.

The previous data show that the GPTMS surface plays a primary role in the grafting process of the particles and that within some limits the surface itself can be used as a chemical switch with on−off response to CeO_2 NPs bonding. This property is directly correlated with the aging of the precursor sol which is used for the deposition, which means with the

proceed of the polycondensation reactions of both the organic (epoxides) and the inorganic species (the silanols). Only when the epoxide has completely reacted (between 2 and 3 days of aging) the film will allow a successful grafting on the surface of the particles. The FTIR data show that with aging and opening of the epoxides more OH species are detected, they are the bonding sites which should favor the grafting between condensation reaction of OH species on the film and surface particles. The increase of hydrophylicity with aging also increases the surface bagnability and the grafting efficiency. Hydrogen bonding also is likely to have an important role in binding the ceria NPs on the hybrid surface; in any case, the bonds should be strong enough to allow a robust grafting but at the same time should allow a controlled releasing of the particles upon controlled conditions.

2.4. Release of Ceria Nanopatricles. To test the release of the particles from the films we have used Raman spectroscopy; we have also tried to apply the UV−vis spectroscopy by measuring the difference in absorbance before and after the release but, because of the small changes to be detected and the uncertainty in the baseline, we have not obtained reliable and reproducible results. We have used, therefore, Raman imaging which has two advantages, the crystalline ceria has only one Raman mode around 465 cm^{-1} due to the symmetric breathing vibrations of the oxygen anions around the cerium cation,[40] furthermore it is possible collecting the spectra in a very specific area in imaging mode. This allows averaging the spectra to obtain a good signal-to-noise ratio of the Raman mode of ceria before and after the release. Figure 9a shows the Raman spectra in the 490−425 cm^{-1} range of ceria nanoparticles grafted on GPTMS film before (black line) and after a release test of 1 h (red line), 5 h (cyan) and 17 h (blue line) in phosphate buffer at pH 7.4. The change of ceria Raman integrated band area as a function of releasing test time (in hours) is reported in Figure 9b; the data are well-fitted using an exponential decay curve. This indicates that the particles are not released immediately after the immersion in the buffer, but it is a time dependent process that can be controlled. Within 17 h of immersion of the film with the grafted ceria nanoparticles around 70% of them are released in the buffer solution. This result shows that this system could be potentially developed for controlled release of ceria nanoparticles in materials such as contact lenses; the overall release process is illustrated in Figure 10.

CONCLUSIONS

Optically transparent hybrid organic−inorganic films using 3-glycidoxypropyltrimethoxysilane as organically modified precursor alkoxide have been synthesized in high pH conditions. The surface properties of these films depend on the aging time of the precursor sol, the surface increases its hydrophilicity with aging; this effect is correlated to the reaction of the epoxides, which proceeds with the time. The film surface shows an excellent capability of grafting ceria nanoparticles but only in the case of samples prepared from an aged sol whose epoxides have been full reacted. The ceria-grafted samples upon immersion in a buffer solution slowly release the ceria nanoparticles, showing that this hybrid system is a potential platform to develop new types of materials for controlled release of free radical scavenger nanoparticles.

ASSOCIATED CONTENT

Supporting Information

FTIR absorption spectra in the range 3600−3120 cm^{-1} of GPTMS hybrid films as a function of the aging time.This material is available free of charge via the Internet at http://pubs.acs.org.

AUTHOR INFORMATION

Corresponding Author

*E-mail: plinio@uniss.it.

Notes

The authors declare no competing financial interest.

REFERENCES

(1) Innocenzi, P.; Kidchob, T.; Yoko, T. *J. Sol−Gel Sci. Technol.* **2005**, *35*, 225−35.
(2) Innocenzi, P.; Brusatin, G.; Guglielmi, M.; Bertani, R. *Chem. Mater.* **1999**, *11*, 1672−79.
(3) Innocenzi, P.; Brusatin, G.; Babonneau, F. *Chem. Mater.* **2000**, *12*, 3726−32.
(4) Alonso, B.; Massiot, D.; Babonneau, F.; Brusatin, G.; Della Giustina, G.; Kidchob, T.; Innocenzi, P. *Chem. Mater.* **2005**, *17*, 3172−80.
(5) Innocenzi, P.; Sassi, A.; Brusatin, G.; Guglielmi, M.; Favretto, D.; Bertani, R.; Venzo, A.; Babonneau, F. *Chem. Mater.* **2001**, *13*, 3635−43.
(6) Templin, M.; Wiesner, U.; Spiess, H. W. *Adv. Mater.* **1997**, *9*, 814−17.
(7) Matejka, L.; Dukh, O.; Brus, J.; Simonsick, W. J., Jr.; Meissner, B. *J. Non-Cryst. Solids.* **2000**, *270*, 34−47.
(8) Figus, C.; Takahashi, M.; Kidchob, T.; Yoko, T.; Piccinini, M.; Casula, M.; Innocenzi, P. *J. Sol-Gel Sci. Technol* **2009**, *52*, 408−14.
(9) Menaa, B.; Takahashi, M.; Innocenzi, P.; Yoko, T. *Chem. Mater.* **2007**, *19*, 1946−53.
(10) Takahashi, M.; Figus, C.; Kidchob, T.; Enzo, S.; Casula, M.; Valentini, M.; Innocenzi, P. *Adv. Mater.* **2009**, *21*, 9146−52.
(11) Innocenzi, P.; Martucci, A.; Guglielmi, M.; Armelao, L.; Battaglin, G.; Pelli, S.; Righini, G. C. *J. Non-Cryst. Solids.* **1999**, *259*, 182−90.
(12) Brusatin, G.; Guglielmi, M.; Innocenzi, P.; Martucci, A.; Battaglin, G.; Pelli, S.; Righini, G. *J. Non-Cryst. Solids* **1997**, *220*, 202−09.
(13) Signorini, R.; Meneghetti, M.; Bozio, R.; Maggini, M.; Scorrano, G.; Prato, M.; Brusatin, G.; Innocenzi, P.; Guglielmi, M. *Carbon* **2000**, *38*, 1653−62.
(14) Innocenzi, P.; Brusatin, G.; Guglielmi, M.; Signorini, R.; Meneghetti, M.; Bozio, R.; Maggini, M.; Scorrano, G.; Prato, M. *J. Sol−Gel Sci. Technol.* **2000**, *19*, 263−66.
(15) Innocenzi, P.; Brusatin, G.; Guglielmi, M.; Signorini, R.; Bozio, R.; Maggini, M. *J. Non-Cryst. Solids* **2000**, *265*, 68−74.
(16) Innocenzi, P.; Miorin, E.; Brusatin, G.; Abbotto, A.; Beverina, L.; Pagani, G. A.; Casalboni, M.; Sarcinelli, F.; Pizzoferrato, M. *Chem. Mater.* **2002**, *14*, 3758−66.
(17) Brusatin, G.; Abbotto, A.; Beverina, L.; Pagani, G. A.; Casalboni, M.; Sarcinelli, F.; Innocenzi, P. *Adv. Funct. Mater.* **2004**, *14*, 1160−66.
(18) Brusatin, G.; Innocenzi, P.; Beverina, L.; Pagani, G. A.; Abbotto, A.; Sarcinelli, F.; Casalboni, M. *J. Non-Cryst. Solids.* **2004**, *345*, 575−79.
(19) Philipp, G.; Schmidt, H. *J. Non-Cryst. Solids.* **1984**, *63*, 283−92.
(20) Kasemann, R.; Schmidt, H.; Wintrich, E. *Mater. Res. Soc. Symp. Proc.* **1994**, *346*, 915−21.
(21) Sanchez, C.; Belleville, P.; Popall, M.; Nicole., L. *Chem. Soc. Rev.* **2011**, *40*, 696−53.
(22) Chen, J.; Patil, S.; Seal, S.; McGinnis, J. F. *Nat. Nanotechnol.* **2006**, *1*, 142−50.
(23) Rzigalinski, B. A.; Danelisen, I.; Strawn, E. T.; Cohen, C. A.; Liang, C. *Nanoparticles for Cell Engineering − A Radical Concept*; Nanotechnologies for the Life Sciences; Wiley: New York, 2007,

(24) Karakoti, A. S.; Monteiro Riviere, N. A.; Aggarwal, R.; Davis, J. P.; Narayan, R. J.; Self, W. T.; McGinnis, J.; Seal, S. *JOM.* **2008**, *60*, 33−37.
(25) Ivanov, V. K.; Usatenko, A. V.; Shcherbakov, A. B. *Russ. J. Inorg. Chem.* **2009**, *54*, 1522−27.
(26) Nagarsenker, M. S.; Londhe, V. Y.; Nadkarni, G. D. *Int. J. Pharm.* **1990**, *190*, 63−71.
(27) Bourlais, C. L.; Acar, L.; Zia, H.; Sado, P. A.; Needham, T.; Leverge, R. *Prog. Retin. Eye Res.* **1998**, *17*, 33−58.
(28) Lutterotti, L.; Gialanella, S. *Acta Mater.* **1998**, *46*, 101−10.
(29) Horcas, I.; Fernandez, R.; Gomez-Rodriguez, J. M.; Colchero, J.; Gomez-Herrero, J; Baro, A. M. *Rev. Sci. Instrum.* **2007**, *78*, 013705−013712.
(30) Innocenzi, P.; Figus, C.; Kidchob, T.; Valentini, M.; Alonso, B.; Takahashi, M. *Dalton Trans.* **2009**, *42*, 9146−52.
(31) Alonso, B.; Massiot, D.; Valentini, M.; Kidchob, T.; Innocenzi, P. *J. Non-Cryst. Solids* **2008**, *354*, 1615−26.
(32) Innocenzi, P. *J. Non-Cryst. Solids* **2003**, *316*, 309−19.
(33) Young, R. A., Ed. *The Rietveld Method*; Oxford University Press: Oxford, U.K., 1993.
(34) Marabelli, F.; Wachter, P. *Phys. Rev. B.* **1987**, *36*, 1238−43.
(35) Petrovsky, V.; Gorman, B. P.; erson, H. U.; Petrovsky, T. *J. Appl. Phys.* **2001**, *90*, 2517−21.
(36) Hernandez-Alonso, M. D.; Hungria, A. B.; Martinez-Arias, A. J.; Coronado, M. *Phys. Chem. Chem. Phys.* **2004**, *6*, 3524−29.
(37) Tsunekawa, S.; Fukuda, T.; Kasuya, A. *J. Appl. Phys.* **2000**, *87*, 1318−21.
(38) Patsalas, P.; Logothetidis, S. *Phys. Rev. B.* **2003**, *68*, 035104.
(39) Goharshadi, E. K.; Samiee, S.; Nancarrow, P. *J. Colloid Interface Sci.* **2011**, *356*, 473−80.
(40) McBride, J. R.; Hass, K. C.; Poindexter, B. D.; Weber, W. H. *J. Appl. Phys.* **1994**, *76*, 2435−41.